
Article:
Kingslake, J., Ely, J.C. orcid.org/0000-0003-4007-1500, Das, I. et al. (1 more author) (2017) Widespread movement of meltwater onto and across Antarctic ice shelves. Nature, 544. pp. 349-352. ISSN 0028-0836

https://doi.org/10.1038/nature22049

Widespread movement of meltwater onto and across Antarctic ice shelves

Jonathan Kingslake[1], Jeremy C. Ely[2], Indrani Das[1] & Robin E. Bell[1]
[1]Lamont-Doherty Earth Observatory, Columbia University, Palisades, New York, USA. [2]Department of Geography, University of Sheffield, Sheffield, UK.

Surface meltwater drains across ice sheets, forming melt ponds that can trigger ice-shelf collapse[1, 2], acceleration of grounded ice flow and increased sea-level rise[3, 4, 5]. Numerical models of the Antarctic Ice Sheet that incorporate meltwater's impact on ice shelves, but ignore the movement of water across the ice surface, predict a metre of global sea-level rise this century[5] in response to atmospheric warming[6]. To understand the impact of water moving across the ice surface a broad quantification of surface meltwater and its drainage is needed. Yet, despite extensive research in Greenland[7, 8, 9, 10] and observations of individual drainage systems in Antarctica[10, 11, 12, 13, 14, 15, 16, 17,] we have little understanding of Antarctic-wide surface hydrology or how it will evolve. Here we show widespread drainage of meltwater across the surface of the ice sheet through surface streams and ponds (hereafter 'surface drainage') as far south as 85° S and as high as 1,300 metres above sea level. Our findings are based on satellite imagery from 1973 onwards and aerial photography from 1947 onwards. Surface drainage has persisted for decades, transporting water up to 120 kilometres from grounded ice onto and across ice shelves, feeding vast melt ponds up to 80 kilometres long. Large-scale surface drainage could deliver water to areas of ice shelves vulnerable to collapse, as melt rates increase this century. While Antarctic surface melt ponds are relatively well documented on some ice shelves, we have discovered that ponds often form part of widespread, large-scale surface drainage systems. In a warming climate, enhanced surface drainage could accelerate future ice-mass loss from Antarctic, potentially via positive feedbacks between the extent of exposed rock, melting and thinning of the ice sheet.

We conducted the first Antarctic-wide survey of visible satellite imagery aimed at constraining the locations and glaciological settings occupied by surface drainage systems between 1947 and 2015 (Methods). These systems typically consist of meltwater ponds connected by surface streams. We identified several hundred (696) such systems on ice shelves and major outlet glaciers distributed around the continent. We restrict our focus here to systems that display evidence for water moving across the surface through streams and ponds, while recognizing that other drainage processes, such as flow through snow or surface sheet flow, could also contribute to the movement of surface water.

Large-scale surface drainage onto and across the Pine Island, Sulzberger, Riiser–Larsen and Shackleton ice shelves, and on several glaciers in the Trans-Antarctic Mountains is previously unreported (Fig. 1). We also identified evidence for surface drainage on the Larsen, Nansen, Nivlisen, Roi Baudouin, George VI and Amery (Fig. 1) ice shelves, where surface streams have been observed[13, 14, 15, 18, 19, 20, 21].

Surface streams exist at latitudes from 64.0° S on the Antarctic Peninsula to 85.2° S on Shackleton Glacier (Figs 1 and 2) and elevations from near sea level to more than 1,300 m above sea level (Figs 2, 3 and 4a). Around two-thirds of streams identified originate on ice flowing more slowly than 120 m yr^{-1} and many are found adjacent to low-albedo areas such as exposed rock that protrudes through the ice sheet (nunataks) and 'blue ice' (Fig. 4b)[11]. Many streams transport water from areas of the ice sheet undergoing surface ablation, into areas that are covered in snow (which is potentially permeable to meltwater; Fig. 1).

Within 600 km of the South Pole, on Shackleton Glacier (Figs 1 and 2) water is transported up to 70 km from the edge of the East Antarctic Plateau (1,350 m above sea level) onto the Ross Ice Shelf (85 m above sea level; Fig. 2; Extended Data Fig. 1). Meltwater is produced at high elevations near rock at the glacier margin and flows through streams (Extended Data Fig. 1), marginal melt ponds (Fig. 2f) and many closely spaced ponds on Swithinbank Moraine (Extended Data Fig. 1). At lower elevations water drains through streams running parallel to surface lineations (Fig. 2e, i). At less than 200 m above sea level streams coalesce to form a braided network that crosses the grounding line (Fig. 2j) and feeds a pond on the Ross Ice Shelf (Fig. 2k; Extended Data Fig. 1a). Other glaciers in the Trans-Antarctic Mountains that support surface drainage systems include the Darwin, Nimrod, Lennox-King and Liv glaciers.

In many systems meltwater originates in ablation areas on the ice-sheet's flanks and flows long distances across ice shelves. For example, on Amery Ice Shelf a complex network of interconnected streams transports water up to 120 km, feeding vast ice-shelf melt ponds, up to 3.5 km wide and 80 km long (Fig. 3 and Extended Data Fig. 2). During December 2014 and January 2015, the largest pond on the ice shelf grew to 56.7 ± 1.2 km^2 in area over 25 days and its downstream margin migrated at up to $3{,}670 \pm 20$ m per day (Fig. 3b, c; Extended Data Fig. 2). This drainage-fed mode of pond formation—involving the accumulation of meltwater from a large catchment via surface drainage—contrasts with in situ ponding of meltwater observed elsewhere in Antarctica[22]. Drainage-fed ponds on ice shelves are common (Fig. 1), for example on Pine Island Ice Shelf (Extended Data Fig. 3).

Antarctic surface meltwater drainage has persisted for decades (Extended Data Fig. 4 and Extended Data Table 2). On Shackleton Glacier, melt features appear in aerial photography from 1960 onwards (Fig. 2; Extended Data Figs 1 and 4) and in satellite imagery in 2002 and 2010 (Fig. 2d–k). Near Roi Baudouin Ice Shelf, aerial photography from 1947 reveals ponds and streams at the grounding line that have persisted for 68 years (Extended Data Fig. 5). Water has regularly drained onto and across Nivlisen[14, 15], George VI[14, 21], Riiser–Larsen (Extended Data Fig. 6), Amery[13, 14], Pine Island (Extended Data Fig. 3) and Ross (Extended Data Fig. 7) ice shelves over the last 40 years (Extended Data Fig. 4; Extended Data Table 2).

Surface albedo is a key control on surface melt in Antarctica[17]. Low-albedo blue ice[11, 23], nunataks and surface debris facilitate melting by increasing the absorption of solar energy[24]. Blue ice forms when snow is entirely removed by wind erosion[25], sublimation or melt, often adjacent to nunataks[26], because rugged terrain promotes high winds and low-albedo rock increases air temperatures[27]. Melting and wind erosion lower the ice surface, enlarging areas of exposed rock, leading to coupling between melting, rock exposure and blue-ice formation.

We found a close spatial association between drainage, blue ice and exposed rock: despite blue ice and exposed rock together occupying only 2.2% of the continent's area, 50% of drainage systems originate within 3.6 km of blue ice and 50% originate within 8 km of exposed rock (Fig. 4b). Further south than 75° S this association is stronger (Extended Data Fig. 8), probably because lower air temperatures restrict melting to areas with relatively low albedo. Coupling between blue ice, exposed rock and melting is not captured by the commonly used regional climate model RACMO2. This may explain why the model greatly underestimates melt rates over Amery Ice Shelf (Fig. 3c) and predicts very low mean January air temperatures at the locations of high-elevation drainage systems at extreme southerly latitudes (Fig. 4a).

Accumulation of locally derived meltwater has triggered ice-shelf collapse in Antarctica's warmest regions[4]. Large-scale transport of meltwater could accelerate mass loss elsewhere on the continent. For example, a feedback is possible between melting, rock

exposure and ice-sheet thinning. As ice thins, more rock will be exposed (Fig. 4c), increasing blue-ice formation and melt, which will enlarge drainage systems (Fig. 4d), increasing delivery of water to ice shelves. If water can access areas vulnerable to hydraulically driven fracture, ice-shelves can collapse, which accelerates upstream thinning[4].

How different parts of Antarctica's surface drainage system will respond to increased surface melting[6] will vary. Rock–melt–thinning feedbacks may be most effective where nunataks exist upstream of ice shelves that, owing to their stress state, are vulnerable to collapse. Elsewhere, such as on Nansen Ice Shelf[20], surface drainage systems deliver meltwater directly into the ocean. How efficiently water is transported depends on changing snow properties and ice-shelf mass balance. Where water flows into snow-covered areas (for example, Fig. 3) snow permeability will control how far water can propagate before soaking into subsurface aquifers[17]. Low ice-shelf slopes (typically 0.001) and complex drainage basin structure (Extended Data Fig. 2) suggest that small changes in ice-shelf thickness could strongly impact drainage efficiency.

Large-scale surface drainage in Antarctica had been considered a rarity. Although the latest ice-sheet models[5] predict that meltwater accumulation on ice shelves will be critical to future ice-sheet stability, these models do not consider the surface drainage of meltwater. We have shown that widespread and persistent surface drainage moves water great distances from grounded ablation areas, onto and across ice shelves, and into areas that otherwise would not experience meltwater accumulation. Large-scale drainage is likely to be a dominant factor in future ice-sheet stability. Improving the representation of ice-sheet surface hydrology in climate and ice-sheet models will be vital for improving predictions of ice-sheet mass balance and sea-level rise.

Methods

Continent-wide survey of satellite imagery and aerial photography

We used the Landsat Image Mosaic of Antarctica (LIMA)[29], individual Landsat tiles, Aster imagery and WorldView imagery, to identify features on the surface of the ice sheet and ice shelves created by surface meltwater drainage between 1947 and 2015. LIMA was the primary data source, with the other sources of imagery supplementing LIMA further south than 82.5° S, where Landsat does not reach, and in a few areas where surface drainage was evident in other imagery but not in LIMA, presumably owing to weather conditions.

LIMA consists of over 1,000 Landsat ETM+ scenes acquired primarily between 1999 and 2003 that have been mosaicked over Antarctica into one, nearly cloud-free image. Images are natural colour and pan-sharpened to a spatial resolution of 15 m. The meltwater-drainage features easiest to identify unequivocally in LIMA were surface streams. These features often appeared darker or more blue in colour than the surrounding ice and we mapped them where their meandering or braided plan-form structure indicated that they were formed by water flow. Where LIMA suggested a drainage feature, but the imagery's spatial resolution was insufficient to unequivocally identify the feature, we inspected higher-resolution WorldView imagery using an online tool (http://applications.pgc.umn.edu/viewers/antarctica/). In many cases this allowed us to see in great detail meltwater-drainage features suggested by LIMA imagery.

We took a conservative approach, discounting linear features that could have been produced by ice flow or wind and meltwater features that are not produced by the movement of water, such as linear ponds, by identifying features as streams only where a feature clearly undulated or meandered in a manner reminiscent of a typical surface stream. This conservative approach means that many additional features exist in LIMA that could potentially be interpreted as evidence of surface drainage.

The timing of satellite imagery acquisition in the year is important. Melting and drainage-system development is often restricted to the warmest parts of the summer and the dates of acquisition of images in LIMA and in the online WorldView archive vary. Our limited temporal coverage leads us to underestimate the extent of surface meltwater drainage in areas where the corresponding LIMA image and the WorldView imagery available online were acquired at a time of year when there is little melt. Future work could study multiple Landsat and WorldView images from every location to better quantify the spatial coverage of surface drainage.

We mapped each end of each water-carved surface drainage network and extracted corresponding ice-surface elevations from the Bedmap2 compilation[30]. We also extracted the ice-surface flow velocity[31] at the upper end of each drainage network. In selected areas we searched archived Landsat and Aster imagery, and US Geological Survey (USGS) aerial photography to characterize changes in drainage during single melt seasons (for example, Fig. 3) and the persistence of surface drainage over decades (for example, Extended Data Fig. 4). We obtained Landsat and Aster imagery from the website EarthExplorer (http://earthexplorer.usgs.gov/) hosted by the USGS and USGS photography from the Univ. of Minnesota's Polar Geospatial Center (PGC) website (http://www.pgc.umn.edu/). WorldView imagery was inspected in the PGC's online tool (http://applications.pgc.umn.edu/viewers/) and in some cases (over Shackleton Glacier) obtained directly from PGC. Extended Data Fig. 4 demonstrates that surface drainage has persisted in several locations for decades, but this figure is far from a comprehensive record of all instances of surface drainage in these locations. Large data gaps, cloud cover and ambiguity as to whether a particular feature is evidence of meltwater drainage mean that many instances of surface meltwater drainage probably remain undetected.

Extended Data Table 1 lists the satellite and aerial imagery used in each figure and provides an identifier for each image. Extended Data Table 2 lists the imagery containing evidence of surface meltwater drainage over the last several decades, plotted in Extended Data Fig. 4.

Digitizing surface drainage features

To digitize surface features on Shackleton Glacier (Fig. 2e) and Amery Ice Shelf (Fig. 3 and Extended Data Fig. 2a), we used the geographic information systems package ArcMap (http://desktop.arcgis.com). Melt-pond area evolution on Amery Ice Shelf was computed by mapping the boundary of the pond from multiple natural-colour pan-sharpened Landsat images. Uncertainties in melt-pond areas were computed as the product of the perimeter of each pond and the resolution of the pan-sharpened imagery (15 m). The rate of migration of the pond's down-ice-shelf margins was computed from the displacement of this margin between images and the time separation of image acquisition. The uncertainty in the migration speed was computed by combining the uncertainty in margin location (15 m) from each grid direction in quadrature (the uncertainty in the time of acquisition is negligible compared to the spatial uncertainty).

Analysis of regional climate model output

The regional climate model RACMO2 simulates atmospheric circulation across Antarctica on a 27-km grid and is forced at the model-domain boundaries by reanalysis data[32]. Model output is available for every day between 1 January 1979 and 31 December 2015. We computed the January-mean air temperature at a height of 2 m above the ground in each grid cell over the period 1979–2015 and displayed its 0 °C contour in Fig. 1. To compute time series of 2-m air temperature at the location of the melt pond on Amery Ice Shelf (Fig. 3) we extracted values corresponding to the closest grid cell in the model output. We also extracted the long-term January-mean 2-m air temperature at the upper end of each stream (Fig. 4a). We find that RACMO2 predicts very cold January 2-m air temperatures in locations where we see persistent drainage systems (Fig. 4a) and hypothesize that this is due to low albedo

surfaces that are not included in the model. Using an alternative RACMO2 output that contains information about surface temperatures important for surface melting (called the 'skin temperature') does not affect this conclusion. The simulated skin temperature is consistently lower than the simulated 2-m temperature used above, with this difference being largest in mountain ranges. For example, over the Trans-Antarctic Mountains the difference in the mean January values of the 2-m air temperature and the skin temperature ranges between 0.2 °C and 6.9 °C.

Comparing order-of-magnitude modelled and observed meltwater on Amery Ice Shelf

For each day of the 2014/15 melt season we integrated the mass of meltwater predicted by RACMO2 over the entire Amery Ice Shelf. In Fig. 3b we plot the cumulative meltwater volume using a water density of 1,000 kg m^{-3}. For the sake of comparison of order-of-magnitude meltwater volumes, we assume that the melt pond depicted in Fig. 3b had a uniform depth of 1 m (close to the mean depth computed for Larsen B Ice Shelf[10], 0.8 m), to compute the 'observed' volumes plotted in Fig. 3b. Upper and lower estimates of lake volume are obtained by assuming a lake depth of 1 cm as a lower bound and 10 m as an upper bound, as well as taking the lower and upper bound on mapped lake areas (taking into account the uncertainty estimated in the mapped lake areas). The vertical lines in Fig. 3c represent the range between these upper and lower bounds.

The melt pond's peak volume is estimated as 4.5×10^7 m^3 (assuming a depth of 1 m), around four orders of magnitude larger than the RACMO2-modelled melt production for the entire Amery Ice Shelf during the same period. Amery Ice Shelf is adjacent to nunataks and is partly covered by blue ice (Extended Data Fig. 2). RACMO2 does not account for spatial variations in albedo and so we hypothesize that the model may not simulate sufficient heat absorption to generate realistic melt rates.

A more precise comparison between modelled and observed melt volumes would use multi-spectral imagery[33, 34] to map the depth of the pond and compute volumes rather than estimate them using an assumed mean depth, as we have done here. A more precise comparison would be worthwhile if it would allow us to compute a water budget for the pond and compute how much water accesses an unobserved englacial drainage system—either a firn aquifer or an englacial system of fractures or conduits. This may be possible in future work using regional climate models that include spatially variable albedo and can realistically simulate melt rates.

Computing proximity to blue ice and exposed rock

Masks of blue ice and exposed rock[26] were produced through calibrated characterization of surface spectral properties determined from Landsat imagery. We used ArcMap to compute the planar distance from the upper end of each mapped drainage system to the nearest rock and to the nearest blue ice. Figure 4b and Extended Data Fig. 8 display the results as a proportion of all the streams that originate within a range of distances of rock and blue ice ($n = 696$).

Estimating increase in exposed-rock area due to ice-sheet thinning

Using the Bedmap2 continent-wide ice thickness data set[30], we estimated the area of the ice sheet that is thinner than a range of values from 0 to 100 m, to estimate how much bedrock would be exposed in response to ice-sheet thinning. Figure 4c plots the total increase in bedrock area and expresses this as a percentage of the current total area of exposed rock. The current total area of exposed rock was determined from the rock mask supplied with Bedmap2. Bedmap2 has a spatial resolution of 1 km. Alternatively, the current area of exposed rock could be computed from the higher resolution (15 m) mask produced from Landsat imagery[26]. If we had ice-thickness data of similarly high spatial resolution, the Landsat-derived mask would yield a more accurate estimate of the impact of thinning on rock exposure. However, as Bedmap2 is the highest-resolution continent-wide ice thickness product available, we instead use the lower-resolution rock mask supplied with this product.

Data availability

The Landsat Image Mosaic of Antarctica (LIMA) can be viewed and downloaded at https://lima.usgs.gov/. Landsat and Aster tiles can be obtained from http://earthexplorer.usgs.gov/. WorldView imagery can either be inspected using the Polar Geospatial Center's (PGC) online tool (http://applications.pgc.umn.edu/viewers/) or obtained by contacting PGC directly. Trimetrogon aerial photography dating from 1947 can be downloaded from http://www.pgc.umn.edu/. Aerial reconnaissance photography is hosted at http://depts.washington.edu/cosmolab/ant_web/shackleton/content/. RACMO2 climate model output can be obtained by contacting the authors of ref. 17 or ref. 32 directly.

References

1. Scambos, T. A., Hulbe, C., Fahnestock, M. & Bohlander, J. The link between climate warming and break-up of ice shelves in the Antarctic Peninsula. J. Glaciol. **46**, 516–530 (2000)
2. Rott, H., Skvarca, P. & Nagler, T. Rapid collapse of northern Larsen ice shelf. Antarct. Sci.**271**, 788–792 (1996)
3. Rignot, E. et al. Accelerated ice discharge from the Antarctic Peninsula following the collapse of Larsen B ice shelf. Geophys. Res. Lett. **31**, L18401 (2004)
4. De Rydt, J., Gudmundsson, G., Rott, H. & Bamber, J. Modeling the instantaneous response of glaciers after the collapse of the Larsen B Ice Shelf. Geophys. Res. Lett. **42**, 5355–5363 (2015)
5. DeConto, R. M. & Pollard, D. Contribution of Antarctica to past and future sea-level rise. Nature **531**, 591–597 (2016)
6. Trusel, L. D. et al. Divergent trajectories of Antarctic surface melt under two twenty-first-century climate scenarios. Nat. Geosci. **8**, 927–932 (2015)
7. Zwally, J. H. et al. Surface melt-induced acceleration of Greenland ice-sheet flow. Science**297**, 218–222 (2002)
8. Das, S. B. et al. Fracture propagation to the base of the Greenland ice sheet during supraglacial lake drainage. Science **320**, 778–781 (2008)
9. Lüthje, M., Pedersen, L. T., Reeh, N. & Greuell, W. Modelling the evolution of supraglacial lakes on the West Greenland ice-sheet margin. J. Glaciol. **52**, 608–618 (2006)
10. Banwell, A. F. et al. Supraglacial lakes on the Larsen B ice shelf, Antarctica, and at Paakitsoq, West Greenland: a comparative study. Ann. Glaciol. **55**, 1–8 (2014)
11. Winther, J. G., Elvehøy, H., Bøggild, C. E., Sand, K. & Liston, G. Melting, runoff and the formation of frozen lakes in a mixed snow and blue-ice field in Dronning Maud Land, Antarctica. J. Glaciol. **42**, 271–278 (1996)
12. Langley, E. S., Leeson, A. A., Stokes, C. R. & Jamieson, S. S. R. Seasonal evolution of supraglacial lakes on an East Antarctic outlet glacier. Geophys. Res. Lett. **43**, 8563–8571 (2016)
13. Phillips, H. A. Surface meltstreams on the Amery Ice Shelf, East Antarctica. Ann. Glaciol.**27**, 177–181 (1998)
14. Swithinbank, C. W. in Satellite Image Atlas of Glaciers of the World: Antarctica (eds Williams, R. S. & Ferrigno, J. G.) USGS Prof. Paper 1386-B (USGS, 1988)
15. Kingslake, J., Ng, F. & Sole, A. Modelling channelized surface drainage of supraglacial lakes. J. Glaciol. **61**, 185–199 (2015)
16. Leeson, A. A. et al. Supraglacial lakes on the Greenland ice sheet advance inland under warming climate. Nat. Clim. Chang. **5**, 51–55 (2015)

17. Lenaerts, J. T. M. et al. Meltwater produced by wind-albedo interaction stored in an East Antarctic ice shelf. Nat. Clim. Chang. **7**, 58–62 (2017)
18. Banwell, A. F., MacAyeal, D. R. & Sergienko, O. V. Breakup of the Larsen B Ice Shelf triggered by chain reaction drainage of supraglacial lakes. Geophys. Res. Lett. **40**, 5872–5876 (2013)
19. Rack, W. & Rott, H. Pattern of retreat and disintegration of the Larsen B ice shelf, Antarctic Peninsula. Ann. Glaciol. **39**, 505–510 (2004)
20. Bell, R. E. et al. Antarctic ice shelf potentially stabilized by export of meltwater in surface river. Naturehttp://dx.doi.org/10.1038/nature22048
21. Reynolds, J. M. Lakes on George VI Ice Shelf, Antarctica. Polar Rec. **20**, 425–432 (1981)
22. Leppäranta, M., Järvinen, O. & Mattila, O.-P. Structure and life cycle of supraglacial lakes in Dronning Maud Land. Antarct. Sci. **25**, 457–467 (2013)
23. Liston, G. E., Bruland, O., Elvehøy, H. & Sand, K. Below-surface ice melt on the coastal Antarctic ice sheet. J. Glaciol. **45**, 273–285 (1999)
24. Box, J. E. et al. Greenland ice sheet albedo feedback: thermodynamics and atmospheric drivers. Cryosphere **6**, 821–839 (2012)
25. Das, I. et al. Influence of persistent wind scour on the surface mass balance of Antarctica. Nat. Geosci. **6**, 367–371 (2013)
26. Hui, F. et al. Mapping blue-ice areas in Antarctica using ETM+ and MODIS data. Ann. Glaciol. **55**, 129–137 (2014)
27. Bintanja, R. & Reijmer, C. H. Meteorological conditions over Antarctic blue-ice areas and their influence on the local surface mass balance. J. Glaciol. **47**, 37–50 (2001)
28. Depoorter, M. A., Bamber, J. L., Griggs, J. A., Lenaerts, J. T. M. & Ligtenberg, S. R. M.Calving fluxes and basal melt rates of Antarctic ice shelves. Nature **502**, 89–92 (2013)
29. Bindschadler, R. et al. The Landsat image mosaic of Antarctica. Remote Sens. Environ. **112**, 4214–4226 (2008)
30. Fretwell, P. et al. Bedmap2: improved ice bed, surface and thickness datasets for Antarctica. Cryosphere **7**, 375–393 (2013)
31. Rignot, E., Mouginot, J. & Scheuchl, B. Ice flow of the Antarctic ice sheet. Science **333**, 1427–1430 (2011)
32. Van Wessem, J. M. et al. Improved representation of East Antarctic surface mass balance in a regional atmospheric climate model. J. Glaciol. **60**, 761–770 (2014)
33. Pope, A. et al. Estimating supraglacial lake depth in West Greenland using Landsat 8 and comparison with other multispectral methods. Cryosphere **10**, 15–27 (2016)
34. Sneed, W. A. & Hamilton, G. Evolution of melt pond volume on the surface of the Greenland Ice Sheet. Geophys. Res. Lett. **34**, L03501 (2007)
35. Haran, T., Bohlander, J., Scambos, T., Painter, T & Fahnestock, M. MODIS Mosaic of Antarctica 2003-2004 (MOA2004) Image Map http://dx.doi.org/10.7265/N5ZK5DM5 (National Snow and Ice Data Center, 2005)

Figures

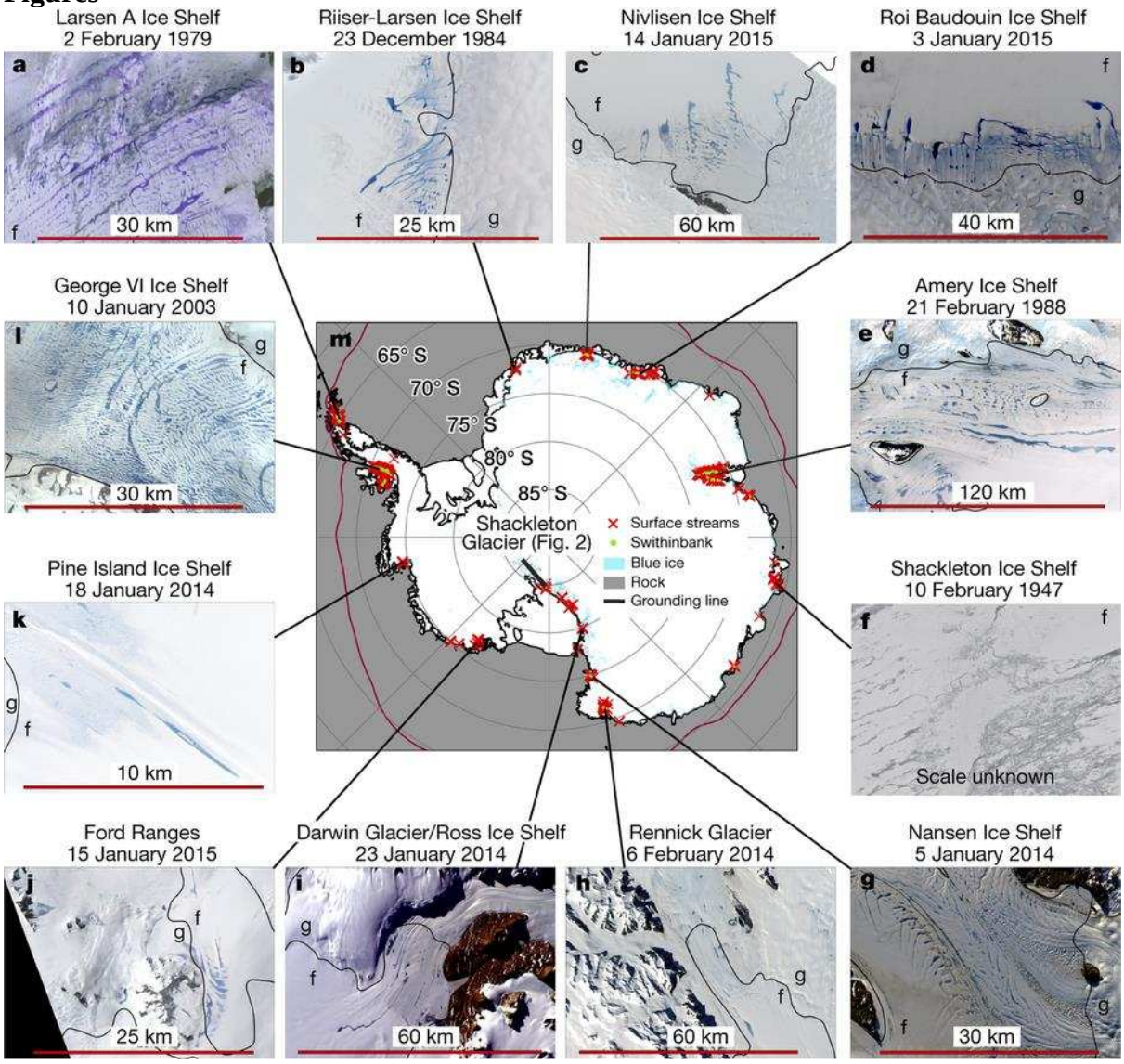

Figure 1: Surface meltwater drainage around Antarctica

a–**l**, Surface drainage systems mapped in this study (red crosses in centre panel **m**) and locations found by an early survey[14] (green dots). All lie within the 0 °C contour of modelled mean January air temperature (red curve; Methods). Panels **a**–**l** show examples of surface drainage systems consisting of streams and ponds (1947–2015) (Extended Data Table 1). In all panels, narrow meandering structures are identified as streams (Methods). The grounding line[28] (black) is the boundary between grounded and floating ice. 'f' and 'g' in the panels distinguish floating and grounded ice. See Extended Data Table 1 for details of imagery.

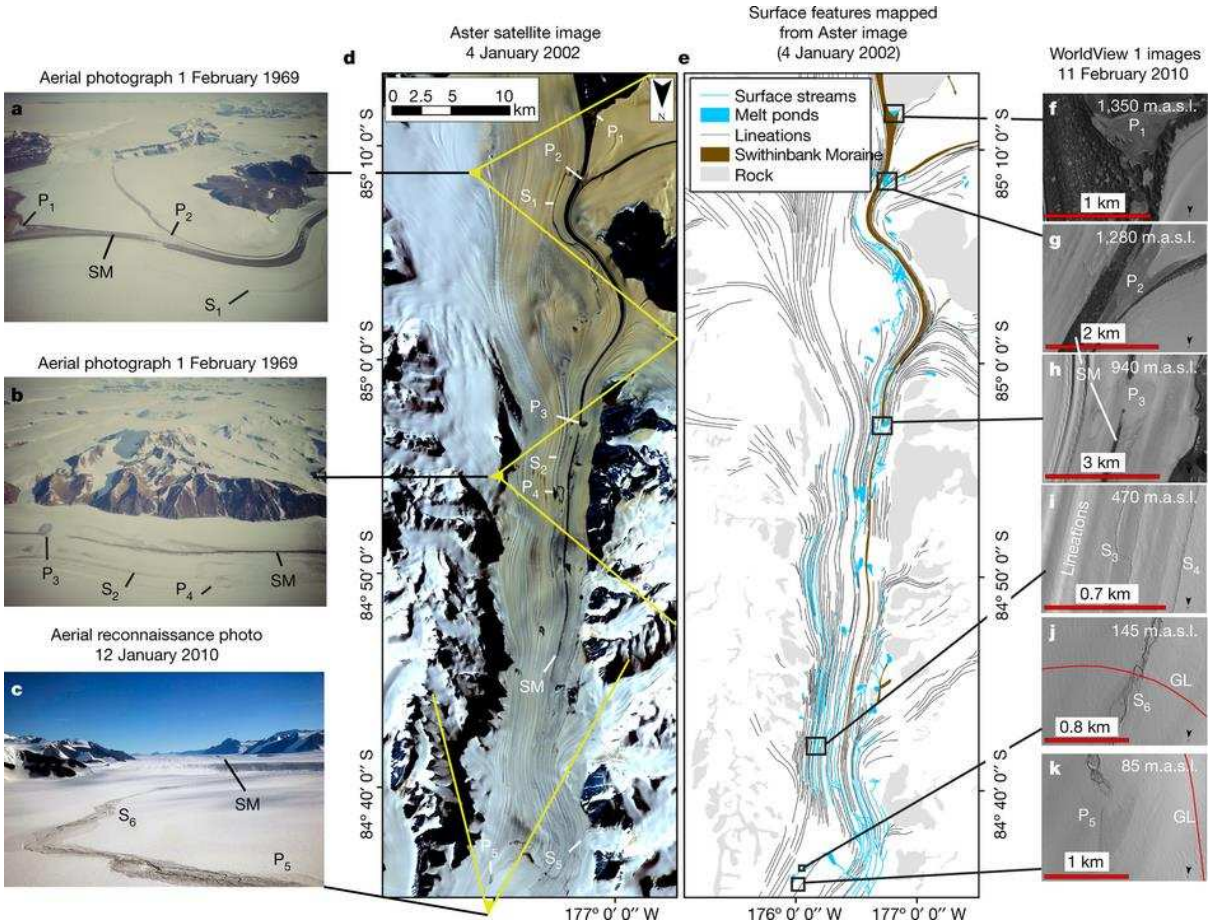

Figure 2: Surface drainage system moves water down Shackleton Glacier onto Ross Ice Shelf

a–**c**, Aerial photographs of streams and ponds. (**c**, Photo credit J. Stone, University of Washington, 2010.) **d**, Aster satellite image with view angles of **a**–**c** shown in yellow; **e**, surface features mapped from **d**. **f**–**k**, WorldView satellite imagery (see Extended Data Table 1 for details). Swithinbank Moraine (SM) and ponds (P_n) and streams (S_n) are visible in each set of imagery. The grounding line (GL) is in red (**j**, **k**). m.a.s.l., metres above sea level.

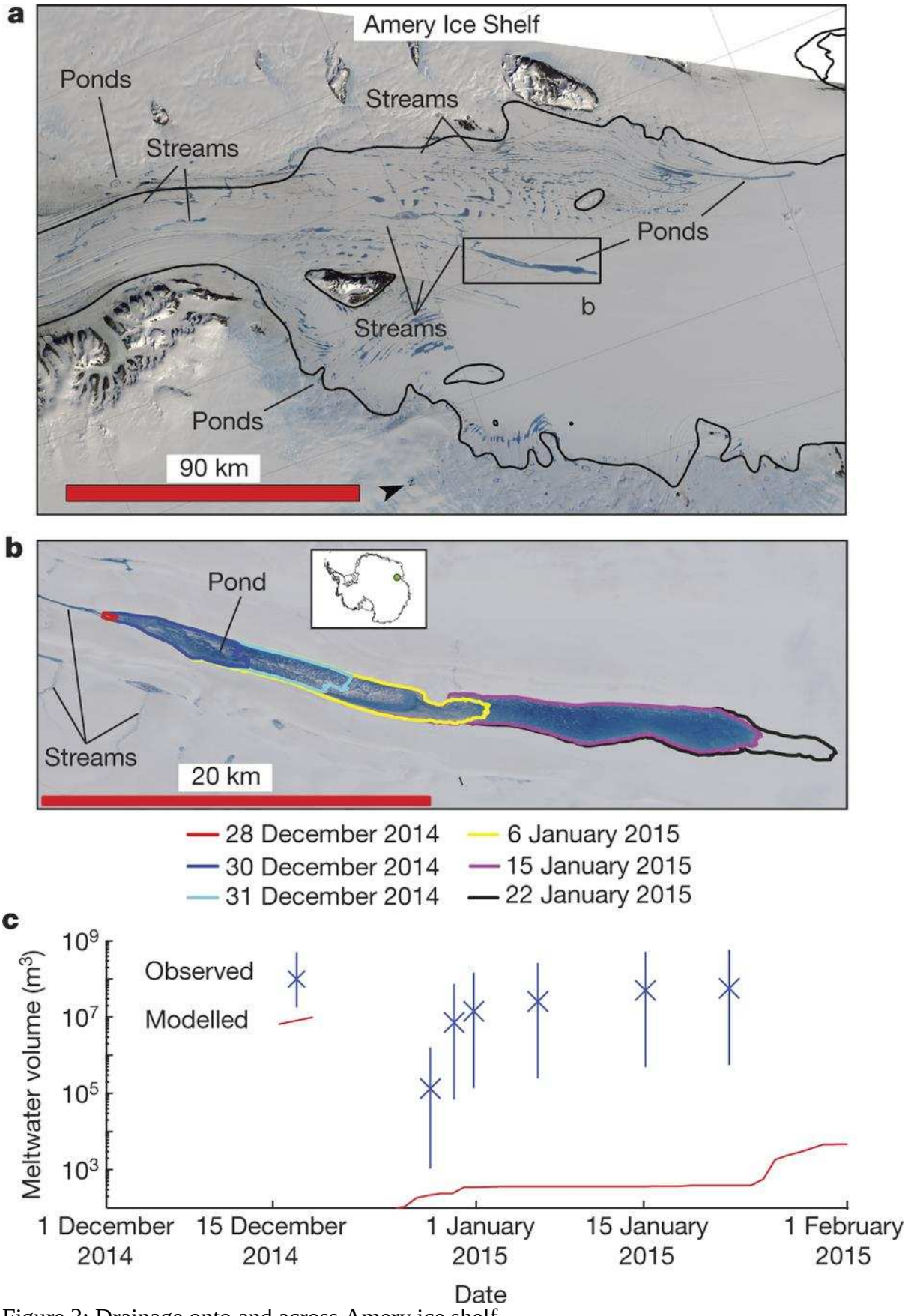

Figure 3: Drainage onto and across Amery ice shelf
a, LANDSAT 8 image from 22 January 2015 showing complex stream networks, barely resolvable at the scale of the image, feeding large meltwater ponds. **b**, The largest pond

observed. It has formed here regularly since at least 1974 (Extended Data Figs 2 and 4). The pond margins are mapped in colour by date (Methods). **c**, Time series of meltwater volume in the pond estimated from imagery assuming 1 m deep water (crosses). Error bars are computed assuming a depth of between 1 cm and 10 m. Melt water production across the entire ice shelf was modelled using RACMO2 (https://www.projects.science.uu.nl/iceclimate/models/racmo.php) (red) (Methods).

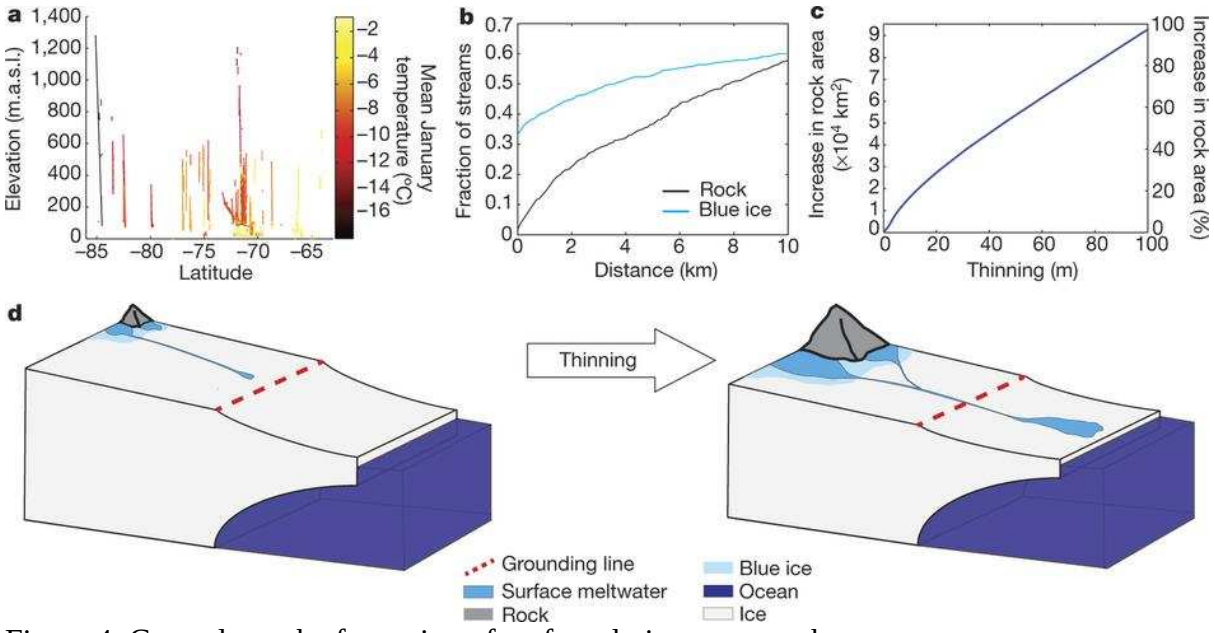

Figure 4: Controls on the formation of surface drainage networks.
a, Elevations and latitudes of drainage systems. Lines connect points corresponding to the upper and lower extremes of each of the 696 surface drainage systems observed (1947–2015). Colours show modelled mean January air temperatures at the upper end of networks (Methods). **b**, Proximity of upper ends of drainage networks to exposed rock (black) and blue-ice (blue) (n = 696). **c**, Total and percentage increase in continent-wide exposed bedrock as a function of ice-sheet thinning (Methods). **d**, Enlarged areas of exposed rock and increased melting caused by ice-sheet thinning, leading to enhanced surface drainage.

Extended Data Table 1. Information on the imagery displayed in all figures. The platform is either the name of the satellite that acquired the imagery (e.g. Landsat, WorldView or Aster), Aerial photography, which refers to the Trimetrogon aerial photography campaigns undertaken by the U.S. Navy starting in 1947, or Reconnaissance photography, which refers to photography taken on a hand-held camera by J. Stone, U. of Washington, during a reconnaissance flight over Shackleton Glacier in 2011. Landsat and Aster imagery can be obtained from http://earthexplorer.usgs.gov/. WorldView imagery can either be inspected using the PGCs online tool (http://applications.pgc.umn.edu/viewers/) or obtained by contacting PGC directly. Trimetrogon aerial photography is hosted at http://www.pgc.umn.edu/. Aerial reconnaissance photography is hosted at http://depts.washington.edu/cosmolab/ant_web/shackleton/content/.

Panel	Location	Platform	Identifier
Fig. 1a	Larsen B Ice Shelf	Landsat 3	LM32311061979032AAA08
Fig. 1b	Riiser-Larsen Ice Shelf	Landsat 5	LT51781111984358XXX03
Fig. 1c	Nivlisen Ice Shelf	Landsat 8	LC81671102015014LGN00
Fig. 1d	Roi Baudouin Ice Shelf	Landsat 8	LC81541102015003LGN00
Fig. 1e	Amery Ice Shelf	Landsat 4	LT41271101988052XXX10,LT41271111988052XXX03
Fig. 1f	Shackleton Ice Shelf	Aerial photography	CA013932V0070
Fig. 1g	Nansen Ice Shelf	Landsat 8	LC82211312014005LGN00
Fig. 1h	Rennick Glacier	Landsat 8	LC80681102014037LGN00
Fig. 1i	Darwin Glacier/Ross Ice Shelf	Landsat 8	LC80021262014023LGN00
Fig. 1j	Ford Ranges/Sulzberger Ice Shelf	Landsat 8	LC80281152015016LGN00
Fig. 1k	Pine Island Ice Shelf	Landsat 8	LC82321132014018LGN00
Fig. 1l	George VI Ice Shelf	Landsat 7	LE72181102003010PFS00
Fig. 2a	Shackleton Glacier	Aerial photography	CA218933R0026
Fig. 2b	Shackleton Glacier	Aerial photography	CA218933R0017
Fig. 2c	Shackleton Glacier	Reconnaissance photography	N/A
Fig. 2d	Shackleton Glacier	Aster	AST_L1T_00301042002162335_20150421034209_32733
Fig. 2f	Shackleton Glacier	WorldView 1	WV01_20100211195819_102001000AD8C300_10FEB11195819
Fig. 2g	Shackleton Glacier	WorldView 1	WV01_20100211195819_102001000AD8C300_10FEB11195819
Fig. 2h	Shackleton Glacier	WorldView 1	WV01_20100211195817_102001000AD8C300_10FEB11195817
Fig. 2i	Shackleton Glacier	WorldView 1	WV01_20100211195816_102001000AD8C300_10FEB11195816
Fig. 2j	Shackleton Glacier	WorldView 1	WV01_20100211195815_102001000AD8C300_10FEB11195815
Fig. 2k	Shackleton Glacier	WorldView 1	WV01_20100211195815_102001000AD8C300_10FEB11195815
Fig. 3a	Amery Ice Shelf	Landsat 8	LC81271102015022LGN00, LC81271122015022LGN00, LC81271112015022LGN00
Fig. 3b	Amery Ice Shelf	Landsat 8	LC81261112015015LGN00
Ext. Fig. 1a	Shackleton Glacier	WorldView 1	WV01_20100211195815_102001000AD8C300_10FEB11195815
Ext. Fig. 1c-1f	Shackleton Glacier	Reconnaissance photography	N/A
Ext. Fig. 2a	Amery Ice Shelf	Landsat 8	LC81271102015022LGN00, LC81271122015022LGN00, LC81271112015022LGN00
Ext. Fig. 2b	Amery Ice Shelf	Landsat 4	LT41271101988052XXX10 and LT41271111988052XXX03
Ext. Fig. 2c	Amery Ice Shelf	Landsat 1	LM11341111974051AAA02
Ext. Fig. 3b	Pine Island Ice Shelf	Landsat 8	LC82321132013335LGN00
Ext. Fig. 3c	Pine Island Ice Shelf	Landsat 8	LC81541322013349LGN00
Ext. Fig. 3d	Pine Island Ice Shelf	Landsat 8	LC82331132013358LGN00
Ext. Fig. 3e	Pine Island Ice Shelf	Landsat 8	LC81581312014012LGN00
Ext. Fig. 3f	Pine Island Ice Shelf	Landsat 8	LC81561312014014LGN00
Ext. Fig. 3g	Pine Island Ice Shelf	Landsat 8	LC82321132014018LGN00
Ext. Fig. 3h	Pine Island Ice Shelf	Landsat 8	LC82311132014027LGN00
Ext. Fig. 5a	Roi Baudouin Ice Shelf	Aerial Photography	CA019400R0074
Ext. Fig. 5b	Roi Baudouin Ice Shelf	Aerial Photography	CA019400R0070
Ext. Fig. 5c	Roi Baudouin Ice Shelf	Aerial Photography	CA019400R0067
Ext. Fig. 5d	Shackleton Glacier	Aerial photography	CA078633R0054
Ext. Fig. 6b	Riiser-Larsen Ice Shelf	Landsat 1	LM11911111974018AAA05
Ext. Fig. 6c	Riiser-Larsen Ice Shelf	Landsat 5	LT51781111984358XXX03
Ext. Fig. 6d	Riiser-Larsen Ice Shelf	Landsat 4	LM41781111988041AAA03
Ext. Fig. 6e	Riiser-Larsen Ice Shelf	Landsat 8	LC81801112014054LGN00
Ext. Fig. 6e	Riiser-Larsen Ice Shelf	Landsat 8	LC81801112014054LGN00
Ext. Fig. 7b	Darwin Glacier/Ross Ice Shelf	Landsat 1	LM10461191974016AAA04
Ext. Fig. 7c	Darwin Glacier/Ross Ice Shelf	Landsat 5	LT50551171984360XXX04
Ext. Fig. 7d	Darwin Glacier/Ross Ice Shelf	Landsat 4	LT40501181989026XXX03
Ext. Fig. 7e	Darwin Glacier/Ross Ice Shelf	Landsat 7	LE70481182001365EDC02
Ext. Fig. 7f	Darwin Glacier/Ross Ice Shelf	Landsat 8	LC80021262014023LGN00

Extended Data Table 2: Additional information on the evidence for surface meltwater drainage over the last nearly 70 years. See also Extended Data Fig. 7. The year supplied below is the year the melt season in which the evidence for surface drainage is observed, ends. In the majority of cases (for the Landsat imagery) the actual date is contained in the identifier. To avoid repetition, if an image has been displayed in a figure, this is indicated and the identifier can be obtained from Extended Data Table 1.

Location	Year	Platform	Identifier of figure number
Shackleton Glacier	1960	Aerial photography	Ext. Fig. 5d
	1969	Aerial photography	Figs. 2a and 2b
	2002	Aster	Fig. 2d
	2010	Reconnaissance photography	Figs. 2c and Ext. Fig. 1
	2011	WorldView 1	Figs. 2f–2k and Ext. Fig. 1
Darwin Glacier/Ross Ice Shelf	1961	Aerial photography	CA074732V0195
	1974	Aerial photography	CA244633R0206
	1974	Landsat 1	Ext. Fig. 7b
	1985	Landsat 5	Ext. Fig. 7c
	1989	Landsat 4	Ext. Fig. 7d
	2002	Landsat 7	Ext. Fig. 7e
	2014	Landsat 8	Fig. 1i and Ext. Fig. 7f
Pine Island Ice Shelf	1990	Landsat 4	LT42321131990024XXX01
	1997	Landsat 5	LT50021131997024XXX01
	2003	Landsat 7	LE72321132003028EDC00
	2005	Landsat 7	LE72331132005024ASN00
	2007	Landsat 7	LE70011132007005ASN00
	2012	Landsat 7	LE72331132012012EDC00
	2013	Landsat 7	LE72311132013016EDC00
	2014	Landsat 8	Fig. 1k and Ext. Fig. 3
	2015	Landsat 8	LC80021132015026LGN00
Amery Ice Shelf	1973	Landsat 1	LM11311111973035AAA05
	1974	Landsat 1	Ext. Fig. 2c
	1988	Landsat 4	Ext. Fig. 2b
	1990	Landsat 4	LT41281111989349XXX02
	2004	Landsat 7	LE71291102004030ASN01
	2005	Landsat 7	LE71291102005016PFS00
	2006	Landsat 7	LE71261112006014EDC00
	2008	Landsat 7	LE71291112008009PFS00
	2009	WorldView 1	10100100091CBA00
	2010	Landsat 7	LE71271112010032SGS00
	2015	Landsat 8	Fig. 3a and Ext. Fig. 2a
Riiser-Larsen Ice Shelf	1974	Landsat 1	Ext. Fig. 6b
	1984	Landsat 5	Ext. Fig. 6c
	1988	Landsat 4	Ext. Fig. 6d
	2010	Landsat 7	LE71801112010019ASN00
	2014	Landsat 8	Ext. Figs. 6e and 6f
Roi Baudouin Ice Shelf	1947	Aerial photography	Ext. Fig. 5
	1974	Landsat 1	LM11661101974028FAK03
	1976	Landsat 2	LM21651101976045AAA04
	2008	Landsat 7	LE71551102008031SGS00
	2009	Landsat 7	LE71551102009017ASN00
	2010	WorldView (GeoEye1)	463195
	2015	Landsat 8	Fig. 1d
George VI Ice Shelf	1973	Landsat 1	LM12321101973009FAK02
	1985	Landsat 5	LM52171101985057AAA03
	1990	Landsat 4	LT42171101990015XXX04
	2003	Landsat 7	LE72181102003026EDC00
	2011	WorldView 1	10200100114BF600
Nivlisen Ice Shelf	1976	Landsat 2	LM21771101976039AAA05
	1988	Landsat 4	LT41671101988012XXX03
	1989	Landsat 4	LT41671101989014XXX04
	1993	Landsat 4	LT41661101993018XXX02
	2001	Landsat 7	LE71651102001001SGS00
	2003	Landsat 7	LE71661102003014SGS00
	2007	Landsat 7	LE71651102007034ASN00
	2008	Landsat 7	LE71651102008005ASN00
	2010	Landsat 7	LE71651102010026ASN00
	2011	WorldView 1	1020010011CE1300
	2013	Landsat 7	LE71641102013027ASN00
	2015	Landsat 8	Fig. 1c
Nansen Ice Shelf	1961	Aerial photography	CA073631L0122
	1974	Landsat 1	LM10641141974016AAA02
	1975	Aerial photography	CA238432V0020
	1992	Landsat 4	LT40631131992030XXX02
	2009	Landsat 7	LE70621132009021EDC00
	2011	WorldView	102001000FC37C00
	2014	Landsat 8	LC82211312014005LGN00

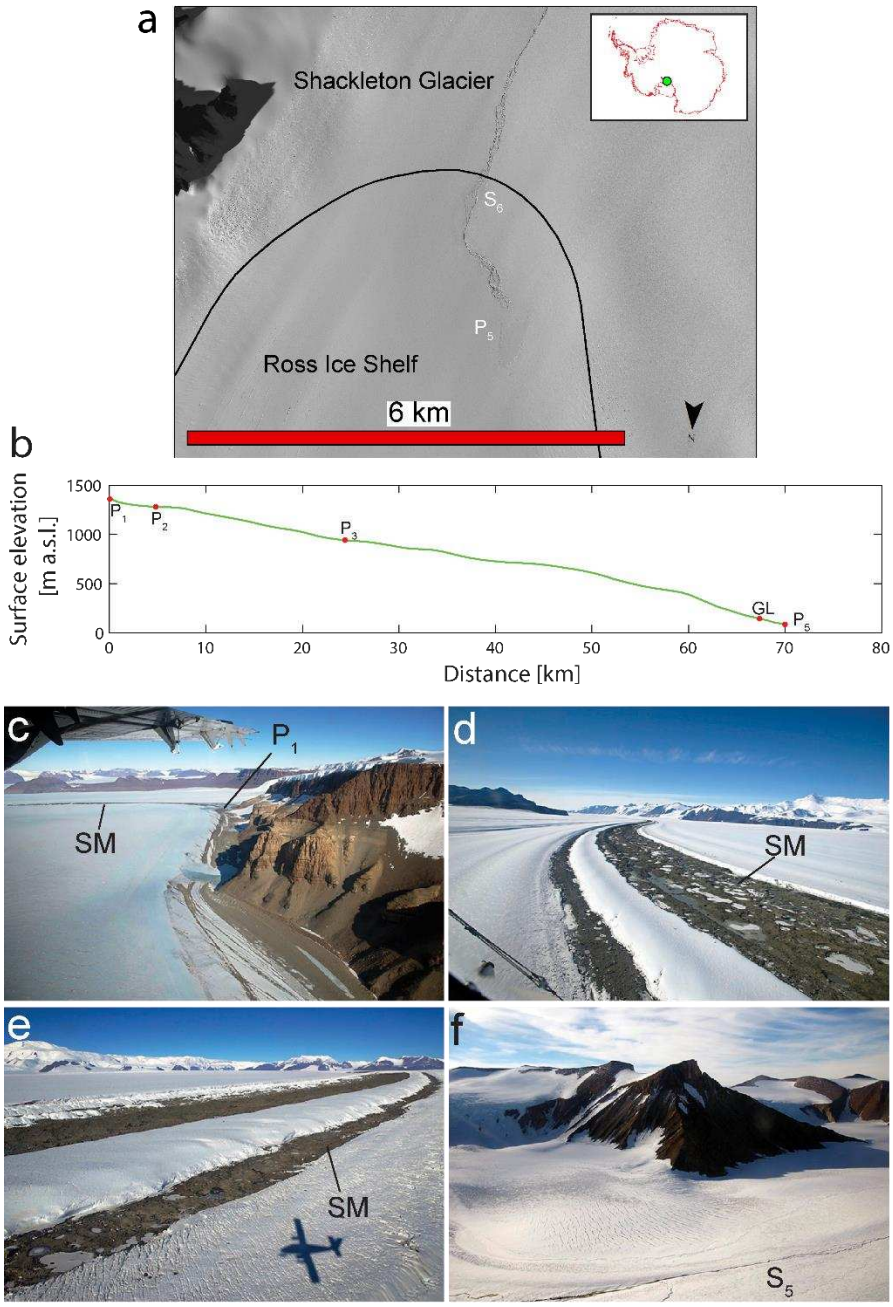

Extended Data Figure 1: Drainage on Shackleton Glacier. (a) WorldView 1 image showing a surface stream flowing from Shackleton Glacier, across the grounding line[Error! Bookmark not defined.] (black), onto the Ross Ice Shelf, from 11th Feb 2010. See also Fig. 2j. (b) Shackleton Glacier surface profile extracted from Bedmap 2 (ref. **Error! Bookmark not defined.**). Ponds labelled in Fig. 2 and the grounding line (GL) are marked. (c) – (f) Aerial reconnaissance photography of meltwater drainage on Shackleton Glacier from 12th Jan 2010, courtesy of J. Stone, U. of Washington. (c) A large pond, P_1, at the head of the Swithinbank Moraine, SM. (d) Smaller meltwater ponds on the surface of SM. (e) Further surface ponding on SM. (f) A meltwater channel, S_5 running parallel to ice flow.

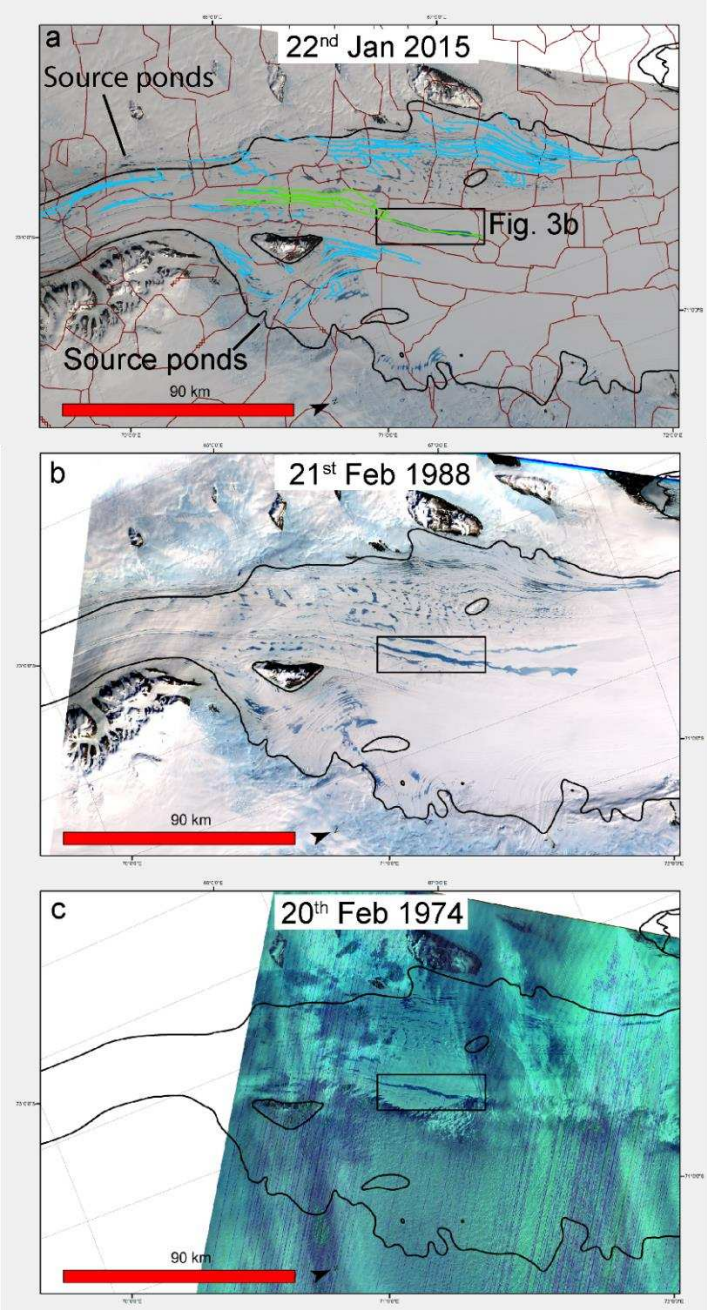

Extended Data Figure 2. Drainage onto and across Amery Ice Shelf. Landsat imagery from (a) 2015, (b) 1988 and (c) 1974. The black boxes show the extent of Fig. 3b. Drainage basins computed from Bedmap2 (ref. **Error! Bookmark not defined.**) are shown in red in (a). The drainage network that feeds the large pond, shown in detail in Fig. 3b, is shown here in green and other major drainage systems shown mapped in blue. See inset in Fig. 3b for location in East Antarctica. Some of the melt ponds on the ice-sheet flank that are the source of ice-shelf streams are labelled source ponds in (a). The grounding line**Error! Bookmark not defined.** is in black.

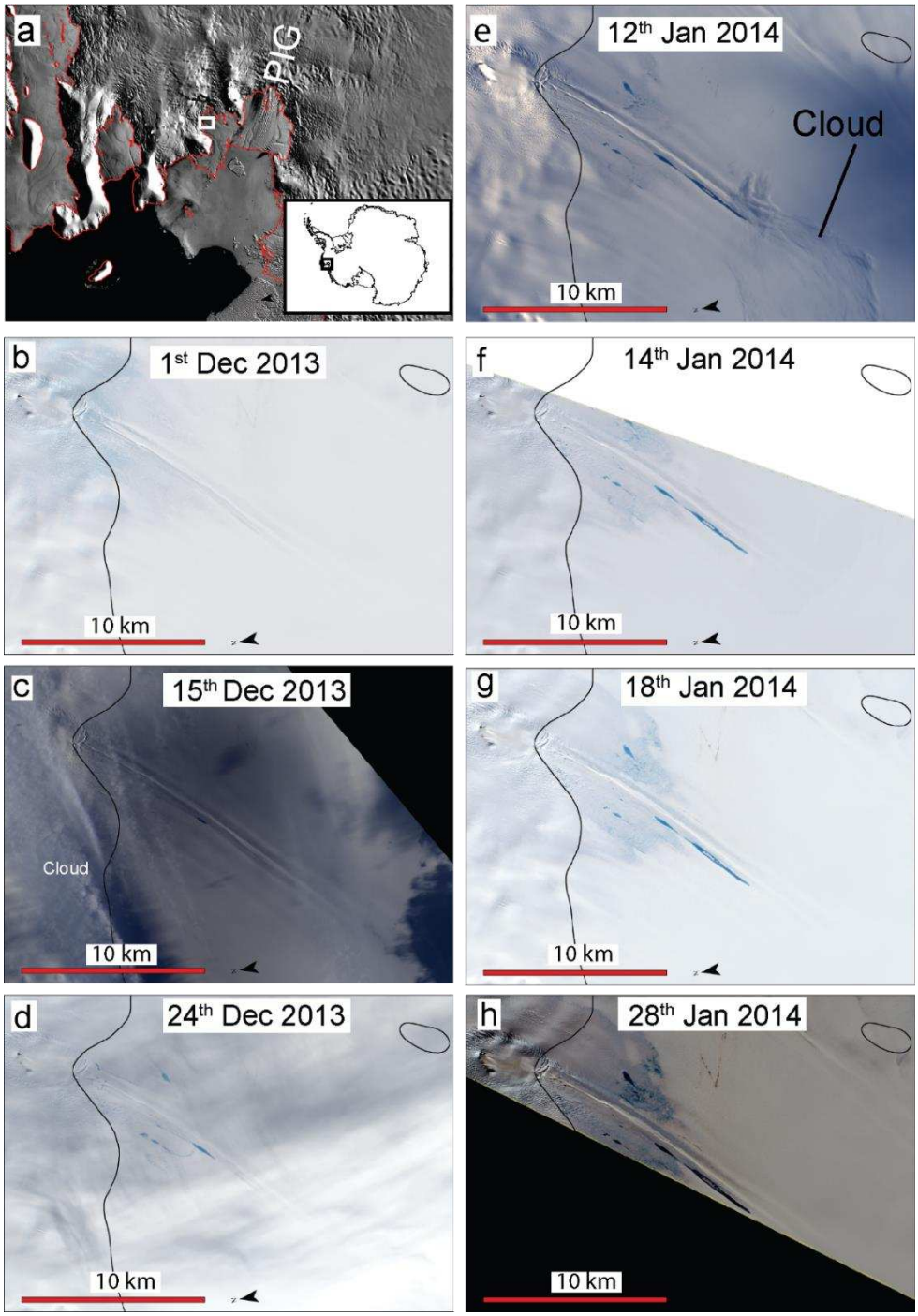

Extended Data Figure 3: Drainage across Pine Island Ice Shelf. (a) MODIS Mosaic of Antarctica (MOA)[Error! Bookmark not defined.] image showing the ice shelf and surroundings, including Pine Island Glacier (PIG). Inset shows location in West Antarctica. White box shows the extent of the images in the other panels. (b) – (h) Satellite imagery showing the growth of a melt pond during the 2013/14 melt season. The grounding line[Error! Bookmark not defined.] is in black.

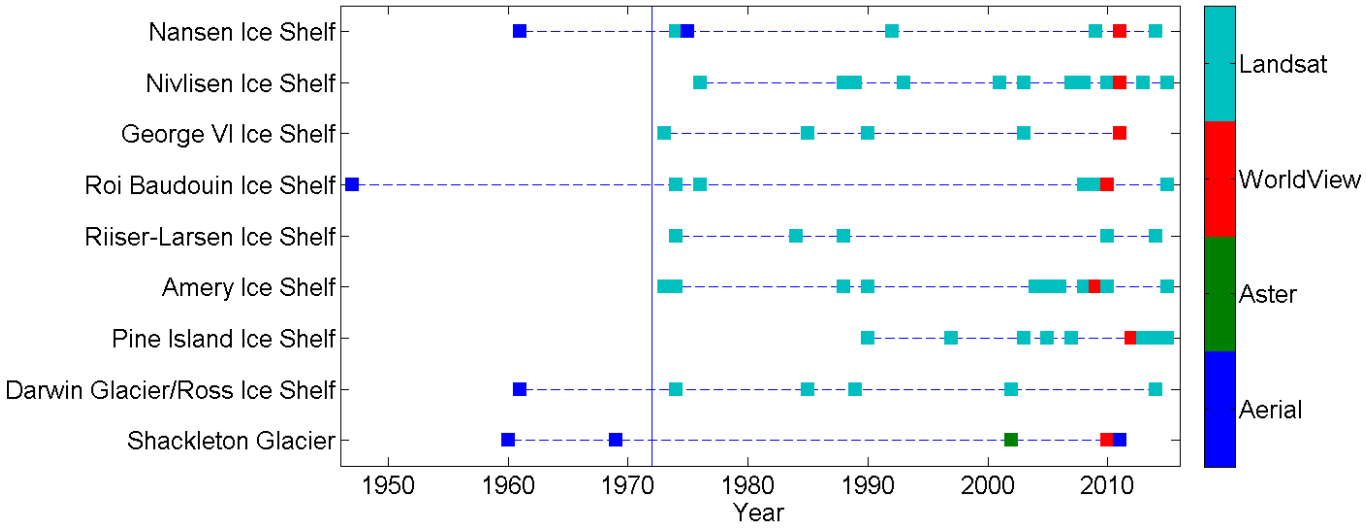

Extended Data Figure 4: Persistence of nine surface drainage systems. Squares show the year of observations of surface drainage in each system. This figure represents a lower bound on the occurrence of drainage in each location. Colors indicate if the observation is from Landsat imagery, WorldView imagery, Aster imagery or aerial photography. The vertical line at 1972 marks the launch of the first Landsat satellite. See Extended Data Table 2 for details.

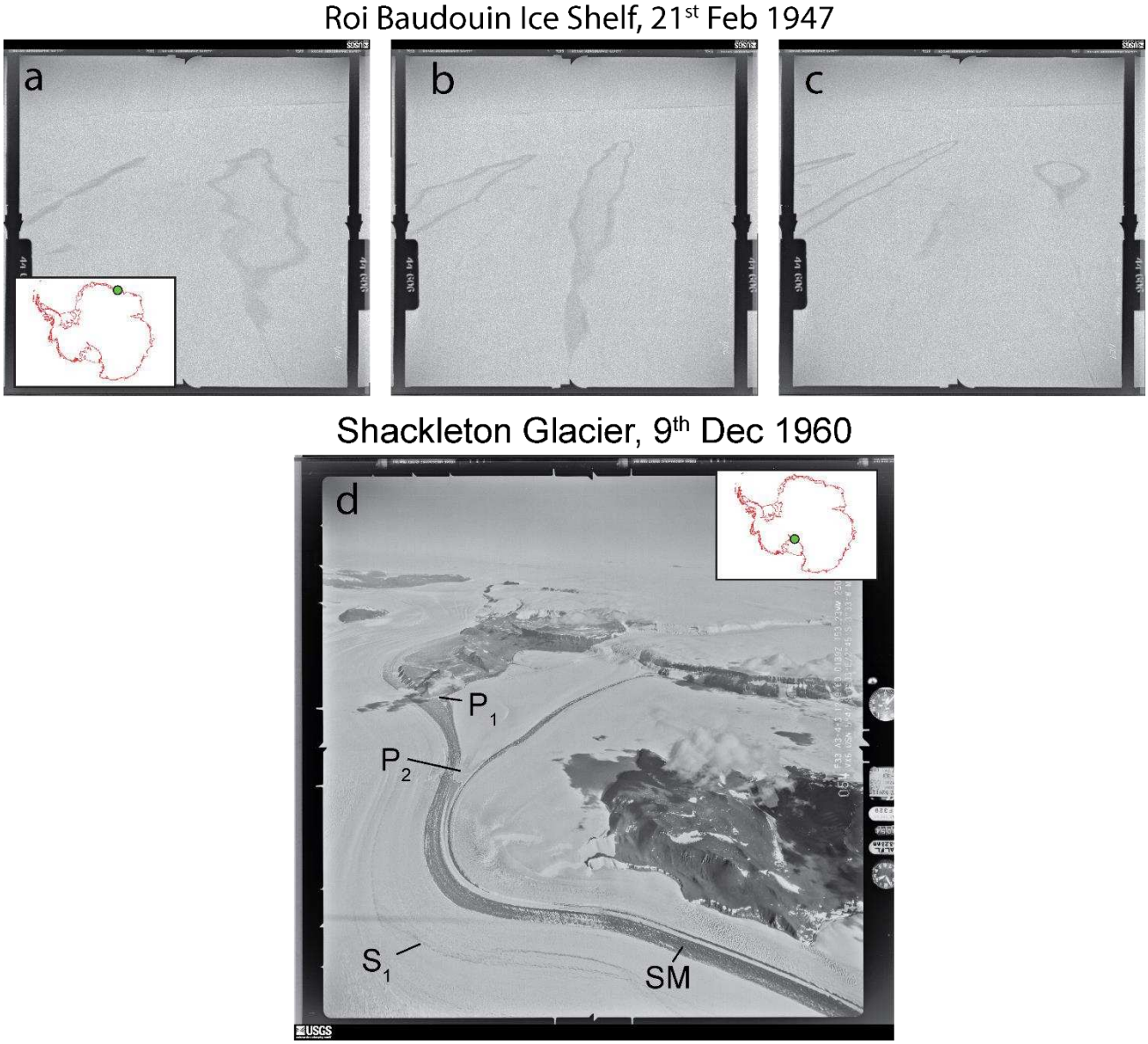

Extended Data Figure 5: **Pre-satellite era aerial photography of persistent surface drainage systems.** (a – c) Oblique aerial photography of melt ponds on Roi Baudouin Ice Shelf, fed by surface streams. Look direction is approximately northwards from the grounding line. The pond that appears on the right in (a) can also be seen in (b) and (c). (d) Aerial photograph of Shackleton Glacier, 9th December 1960, showing meltwater features P_1, P_2 and S_1, that are visible in more recent satellite imagery and aerial photographs (Fig. 2).

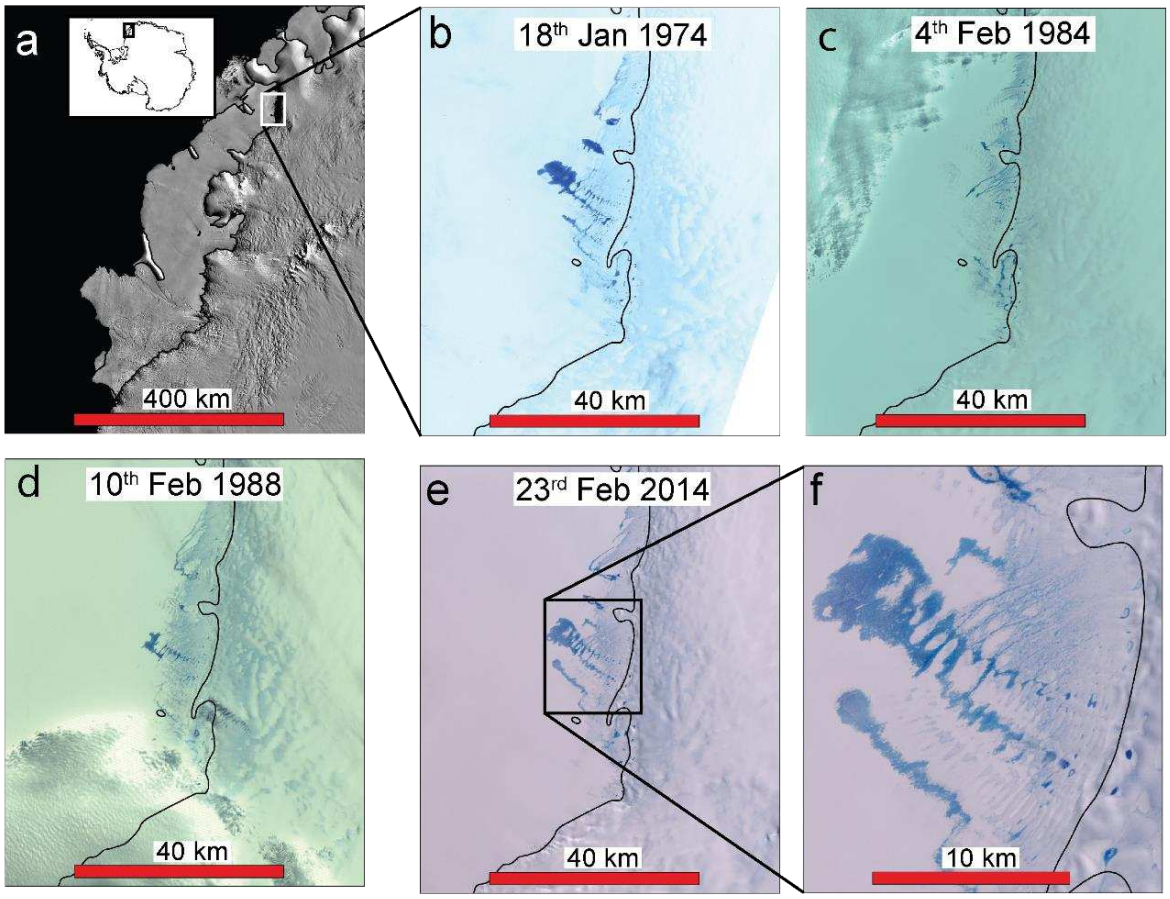

Extended Data Figure 6: Surface drainage across Riiser-Larsen Ice Shelf. (A) White box shows the location of the images shown in the other panels. Background image is from MOA. The inset shows the location in East Antarctica. (b) – (e) Landsat images from 1974, 1984, 1988 and 2014. (f) Enlarged view of melt ponds in (e). In all panels the grounding line**Error! Bookmark not defined.** is in black.

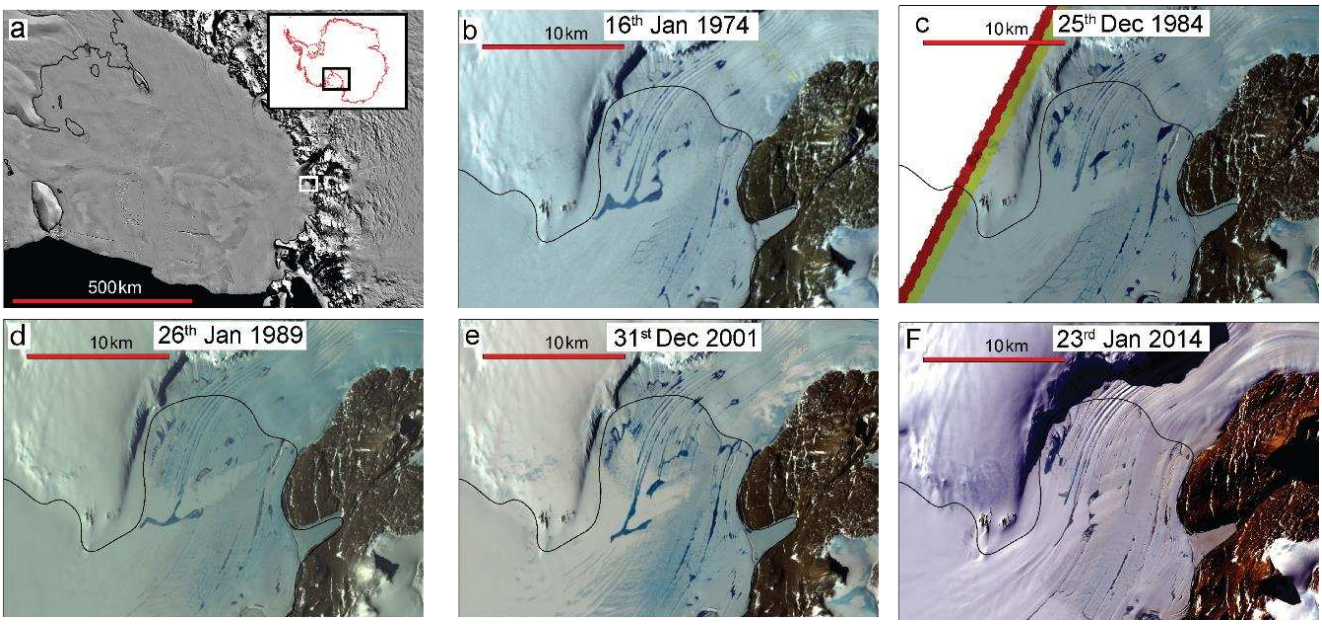

Extended Data Figure 7: Drainage on Ross Ice Shelf, downstream of Darwin Glacier. (a) The location of the other panels is shown in white, background image is from MOA. Inset shows location in Antarctica. (b) - (f) Landsat satellite images showing meltwater ponding and drainage crossing the grounding line**Error! Bookmark not defined.** shown in black, over a 40-year period.

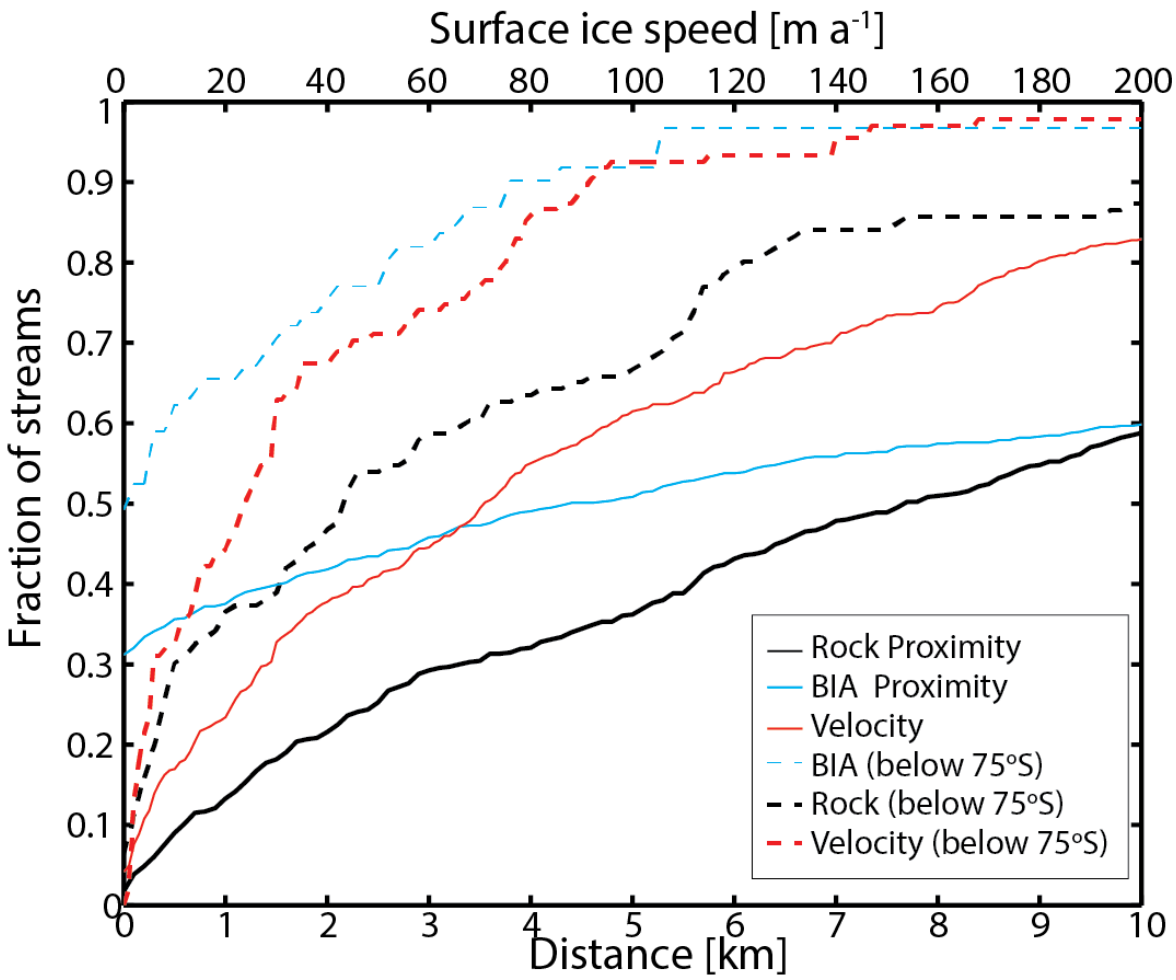

Extended Data Figure 8: **Ice-flow speed and proximity to rock and blue ice at surface streams.** Proximity of upper ends of streams to exposed rock (black) and blue-ice areas (blue) and ice-flow speed at the surface at the upper end of the streams, across the entire continent (solid curves) and further south than 85° (dashed curves) (n = 696).